Available online at www.sciencedirect.com
SCIENCE DIRECT®
International Journal of Thermal Sciences 43 (2004) 1011–1023
International Journal of Thermal Sciences
www.elsevier.com/locate/ijts

Numerical analysis of thermal turbulent flow in the bowl-in-piston combustion chamber of a motored engine

Horng-Wen Wu *, Shiang-Wuu Perng

Department of System and Naval Mechatronic Engineering, National Cheng Kung University, Tainan, 701, Taiwan, ROC

Received 1 April 2003; accepted 2 February 2004

Available online 12 May 2004

Abstract

A numerical analysis of transient turbulent thermal flow has been presented for the bowl-in-piston combustion chamber in a motored engine employing the Large Eddy Simulation which was implemented into the SIMPLE-C algorithm coupled with pre-conditioned conjugate gradient methods. The operating conditions for an engine are changed by various compression ratios (taken as 6.8, 8.7, and 10.6) and initial swirl ratios (taken as 1.325, 5.3, and 9.5) at an engine speed of 900 rpm. The results show that increasing the compression ratio, or the initial swirl ratio obviously makes radial flow (squish) and rotating flow (swirl) stronger as well as enhances the surface heat flux of wall boundaries in the combustion chamber when both of the intake and exhaust valves are closed. Furthermore, the decay rate of normalized angular momentum in the combustion chamber has been analyzed by changing compression ratio or initial swirl ratio.

Keywords: Numerical analysis; Turbulent thermal flow; Bowl-in-piston; Combustion chamber

1. Introduction

The phenomena in reciprocating internal combustion engines are very complicated. Many physical and chemical processes occur and act on each other in complex geometry. Among these processes flow plays an important role for fuel-air mixing, wall heat transfer, and engine performance improvement, so the ability to predict the magnitude of the heat transfer between the working fluid and combustion chamber walls is very important to the designers. There are many parameters that affect internal flow and wall heat flux of an engine, such as engine speed, load, material, initial swirl ratio, compression ratio, turbulent transport, and geometry of the combustion chamber [1–3].

There are several studies conducted on the bowl piston of combustion chamber to predict fluid flow and heat transfer using numerical methods [4,5]. Most investigators confirmed that the shape of the combustion chamber would influence engine performance, but few investigated the influence of interaction between squish and swirl motion on the wall heat transfer. The purpose of this paper is to qualitatively understand the influence of compression ratio and initial swirl ratio on squish motion, swirl motion, and transient heat transfer in the combustion chamber when both intake and exhaust valves are closed. Besides, the decay of swirl in the cylinder is investigated for promoting the mixing of fuel and air in the bowl piston engines in this paper.

This study investigates transient turbulent heat transfer due to a combination of vortex and squish generated by the bowl piston employing the SIMPLE-C algorithm [6] with Large Eddy Simulation [7]. Second-Order Backward Euler (SBE) method [8] is implemented for discretizing the transient term to remove stability restrictions and Extended Linear Upwind Differencing (ELUD) method [9] (third-order scheme) for discretizing the convection terms to avoid severe oscillations. Also, the iterative solution methods based on the pre-conditioned conjugate gradient methods [10,11] were incorporated into the solving process with second-order time advancement. For mesh generation, the time-independent grid system [12] is used for constructing a local computational region attached to the moving boundary (moving piston) and obtaining faster convergence, so it generally requires less computer storage and computation time than the conventional method with the single-grid system at various crank angles. The results of this study

* Corresponding author.
E-mail address: z7708033@email.ncku.edu.tw (H.-W. Wu).

1290-0729/$ – see front matter
doi:10.1016/j.ijthermalsci.2004.02.001

Nomenclature

a	coefficient in the pressure-correction equation
b	mass source in the pressure-correction equation
BDC	bottom dead center (ABDC: after BDC; BBDC: before BDC)
C	length of clearance volume ..... m
C_I	SGS model variable in LES, $= 0.094$
C_P	specific heat of fluid at constant pressure, $= 1.1055\ \text{kJ}\cdot\text{kg}^{-1}\cdot\text{K}^{-1}$ for an ideal gas
C_S	Smagorinsky constant
CR	compression ratio
D	bowl diameter ..... m
E	empirical coefficient used for the wall function, $= 9.0$
E_{SGS}	subgrid-scale kinetic energy ..... $\text{m}^2\cdot\text{s}^{-2}$
f_μ	Van Driest wall damping function $([1-\exp(-Y^+/25)^3]^{1/2})$
G	grid filter function
H	bowl depth ..... m
(H)	the maximum value of the swirl velocity profile in the cylinder ..... $\text{m}\cdot\text{s}^{-1}$
h	enthalpy ..... $\text{kJ}\cdot\text{kg}^{-1}$
L	characteristic length scale ..... m
(L)	the minimum value of the swirl velocity profile in the cylinder ..... $\text{m}\cdot\text{s}^{-1}$
M_P	mass residual of pressure-correction equation ..... kg
N_{rpm}	engine speed ..... rpm
P	pressure ..... Pa
P'	pressure correction ..... Pa
$\widehat{P}$	summation of $\widetilde{P}$ and $2\bar{\rho}E_{\text{SGS}}/3$ ..... Pa
Pr	Prandtl number
Pr_T	turbulent Prandtl number
q_w	wall heat flux ..... $\text{W}\cdot\text{m}^{-2}$
R	computational domain
S	modified factor of temperature boundary layer model
S^+	dimensionless modified factor, $\equiv S\nu/q_w U^*$
S_{ij}	strain rate tensor of the flow field, $= (\partial u_i/\partial x_j + \partial u_j/\partial x_i)/2$ ..... s^{-1}
S_Φ	source term for variable
SR_o	initial swirl ratio ((initial swirl velocity)/$(2\pi r N_{\text{rpm}}/60)$)
SR_m	volume-averaged swirl ratio $((\int_0^{Z_{\text{pis}}}\int_0^r u_\theta r^2\,\text{d}r\,\text{d}z)/((2\pi N_{\text{rpm}}/60)\int_0^{Z_{\text{pis}}}\int_0^r r^3\,\text{d}r\,\text{d}z))$
t	time ..... s
T	temperature ..... K
T^+	dimensionless temperature, $\equiv \bar{\rho}C_P(\widetilde{T}-T_W)U^*/q_w$
T_w	wall temperature ..... K
TDC	top dead center (ATDC: after TDC; BTDC: before TDC)
u_r, u_z, u_θ	velocity components along r, z, and θ axes ..... $\text{m}\cdot\text{s}^{-1}$
U^*	friction velocity, $\equiv\sqrt{\tau_w/\bar{\rho}}$ ..... $\text{m}\cdot\text{s}^{-1}$
U^+	dimensionless velocity, $\equiv\widetilde{U}/U^*$
$\widetilde{U}$	filtered velocity component parallel to the wall ..... $\text{m}\cdot\text{s}^{-1}$
$\vec{V}$	velocity vector ..... $\text{m}\cdot\text{s}^{-1}$
x_i	cylindrical coordinates ($i=1$ for radial coordinate r; $i=2$ for axial coordinate z; $i=3$ for azimuthal coordinate θ)
y	near-wall distance ..... m
Y^+	dimensionless distance from the wall, $\equiv yU^*/\nu$
z_{pis}	the z-coordinate of piston faces ..... m
$\overline{\Delta}$	grid-filter width ..... m
Φ	general dependent flow variable
Φ'	subgrid-scale component of Φ
Φ''	fluctuating quantity of Φ
κ	Von Karman constant
Γ_Φ	diffusion coefficient
μ_{lam}	laminar dynamic viscosity ..... $\text{kg}\cdot\text{m}^{-1}\cdot\text{s}^{-1}$
μ_{turb}	turbulent dynamic viscosity ..... $\text{kg}\cdot\text{m}^{-1}\cdot\text{s}^{-1}$
μ_{eff}	effective dynamic viscosity ..... $\text{kg}\cdot\text{m}^{-1}\cdot\text{s}^{-1}$
ν	laminar kinematic viscosity ..... $\text{m}^2\cdot\text{s}^{-1}$
ν_T	eddy viscosity ..... $\text{m}^2\cdot\text{s}^{-1}$
ρ	density ..... $\text{kg}\cdot\text{m}^{-3}$
Ω	angular momentum of the whole swirl about the cylinder axis ..... $\text{kg}\cdot\text{m}^2\cdot\text{s}^{-1}$
Ω_o	initial value of Ω
Ω^*	ratio of Ω to Ω_o (normalized angular momentum)
τ_w	wall shear stress ..... $\text{kg}\cdot\text{m}^{-1}\cdot\text{s}^{-2}$
θ	crank angle ..... deg
ξ	natural coordinate in computational domain

Superscripts

n	iteration number
—	spatial grid filter indication
$\sim$	Favre-filtered indication

Subscripts

nb	neighbor points of control volume
i, j	indication of components
r, z, θ	indication of cylindrical coordinate components

may be of interest to engineers devoted to flow-modification aspects of heat transfer in the combustion chamber.

2. Physical formulation

The thermal flow field to be simulated is a transient, axial-symmetrical and turbulent flow. Calculation of the reciprocating thermal flow field in an engine requires obtaining the solution of the governing equations.

In Large Eddy Simulation (LES) the flow variables are decomposed into a large-scale component, denoted by an over-bar, and a subgrid-scale component. The large-scale component is defined by the filtering operation:

$$\overline{\Phi}(x_i,t)=\int_R G(x_i-\xi)\Phi(\xi)\,\mathrm{d}\xi,\quad \Phi=\overline{\Phi}+\Phi' \tag{1}$$

where the integral is extended over the entire domain R and G is the grid filter function. The length associated with G is the grid-filter width $\overline{\Delta}$. For variable density flow, utilizing the Favre-filtered (or density-weighted) operation to treat the flow variables is necessary; the variables are then decomposed as followed:

$$\widetilde{\Phi}=\frac{\overline{\rho\Phi}}{\bar{\rho}},\quad \Phi=\widetilde{\Phi}+\Phi'' \tag{2}$$

The transport equations representing the conservation of mass, momentum and thermal energy are cast into a general form of time-dependent and axial-symmetrically cylindrical coordinates, and the governing transport equations filtered by a simple volume-averaged box filter are:

$$\frac{\partial(\bar{\rho}\widetilde{\Phi})}{\partial t}+\frac{1}{r}\left[\frac{\partial}{\partial z}\left(\bar{\rho}\tilde{u}_z r\widetilde{\Phi}\right)+\frac{\partial}{\partial r}\left(\bar{\rho}\tilde{u}_r r\widetilde{\Phi}\right)\right]=\frac{1}{r}\left[\frac{\partial}{\partial z}\left(r\Gamma_\Phi\frac{\partial\widetilde{\Phi}}{\partial z}\right)+\frac{\partial}{\partial r}\left(r\Gamma_\Phi\frac{\partial\widetilde{\Phi}}{\partial r}\right)\right]+S_\Phi(z,r) \tag{3}$$

where Φ represents one of the following entities: 1, u_r, u_z, u_θ, or h in which the dependent variables are radial velocity u_r, axial velocity u_z, swirl velocity u_θ, and enthalpy h. Also, t is time, ρ denotes density, and Γ_Φ and S_Φ stand for the corresponding effective diffusion and source term, respectively. The corresponding expressions of Γ_Φ and S_Φ are given in Table 1. In Eq. (3), the notation $\Phi=1$ denotes the continuity equation.

In Table 1, μ_{lam} is the laminar dynamic viscosity and calculated by the Sutherland law [13], μ_{eff} is the effective dynamic viscosity, P is pressure, T is temperature, and C_P is the specific heat at constant pressure. Subgrid-scale kinetic energy E_{SGS} is calculated according to the paper presented by Yoshizawa and Horiuti [14]. Assuming the fluid to be an ideal gas with constant C_P, we simplify the energy equation by neglecting internal heat generation, radiation heat flux, and energy source [15].

The conventional Smagorinsky subgrid-scale (SGS) model [16] is used to obtain the eddy viscosity as following:

$$\nu_T=L^2\times\sqrt{2\times\widetilde{S}_{ij}\widetilde{S}_{ij}},\quad L=C_S\times\overline{\Delta} \tag{4}$$

where L is a characteristic length scale of small eddies, C_S is Smagorinsky constant ($C_S=0.1$), $\overline{\Delta}$ is the grid-filter width ($\overline{\Delta}=(\Delta r\,\Delta z)^{1/2}$) and $\widetilde{S}_{ij}$ is the strain rate tensor of the filtered flow field. $\widetilde{S}_{ij}$ is expressed as

$$\widetilde{S}_{ij}=\frac{1}{2}\left(\frac{\partial\tilde{u}_i}{\partial x_j}+\frac{\partial\tilde{u}_j}{\partial x_i}\right) \tag{5}$$

During initial runs of the present research, we discovered that the conventional Smagorinsky SGS model did not generate appropriate levels of eddy viscosity in the complex physical domain. For this reason, the Van Driest wall damping SGS model [17] is used here as follows:

$$\nu_T=L^2\times\sqrt{2\times\widetilde{S}_{ij}\widetilde{S}_{ij}},\qquad L=C_S f_\mu\overline{\Delta}$$
$$f_\mu=\left[1-\exp\left(-Y^+/25\right)^3\right]^{1/2} \tag{6}$$

where C_S is equal to 0.15 [18], f_μ is the Van Driest wall damping function, and $Y^+\equiv yU^*/\nu$. The Van Driest wall damping function is used to account for the near wall effect.

This study utilizes the no-slip boundary conditions for velocities at all walls. At the piston crown, the axial velocity $\tilde{u}_z$ is assumed to equal the moving velocity of the piston. Flow field in the near-wall region is matched to boundary layer model. According to the data utilized by Kondoh et al. [4], the air is compressed from 48.5° ABDC to 120°

Table 1
Definition of Φ, Γ_Φ and S_Φ

Φ	Γ_Φ	S_Φ
1	0	0
u_r	μ_{eff}	$-\frac{\partial\widehat{P}}{\partial r}+\frac{\partial}{\partial z}\left(\mu_{\mathrm{eff}}\frac{\partial\tilde{u}_z}{\partial r}\right)+\frac{\partial}{r\partial r}\left(r\mu_{\mathrm{eff}}\frac{\partial\tilde{u}_r}{\partial r}\right)+\frac{\bar{\rho}\tilde{u}_\theta^2}{r}-2\frac{\mu_{\mathrm{eff}}\tilde{u}_r}{r^2}-\frac{2}{3}\frac{\partial}{\partial r}\left(\mu_{\mathrm{eff}}\nabla\cdot\widetilde{\vec{V}}\right)$
u_z	μ_{eff}	$-\frac{\partial\widehat{P}}{\partial z}+\frac{\partial}{\partial z}\left(\mu_{\mathrm{eff}}\frac{\partial\tilde{u}_z}{\partial z}\right)+\frac{\partial}{r\partial r}\left(r\mu_{\mathrm{eff}}\frac{\partial\tilde{u}_r}{\partial z}\right)-\frac{2}{3}\frac{\partial}{\partial z}\left(\mu_{\mathrm{eff}}\nabla\cdot\widetilde{\vec{V}}\right)$
u_θ	μ_{eff}	$-\bar{\rho}\frac{\tilde{u}_\theta\tilde{u}_r}{r}-\frac{\partial}{r\partial r}\left(r\mu_{\mathrm{eff}}\frac{\tilde{u}_\theta}{r}\right)+\mu_{\mathrm{eff}}\frac{\partial(\tilde{u}_\theta/r)}{\partial r}$
h	$\left(\frac{\mu}{Pr}\right)_{\mathrm{eff}}$	$\frac{\mathrm{D}\widehat{P}}{\mathrm{D}t}+\mu_{\mathrm{eff}}\left\{2\left[\left(\frac{\partial\tilde{u}_r}{\partial r}\right)^2+\left(\frac{\partial\tilde{u}_z}{\partial z}\right)^2+\left(\frac{\tilde{u}_r}{r}\right)^2\right]+\left(\frac{\partial\tilde{u}_r}{\partial z}+\frac{\partial\tilde{u}_z}{\partial r}\right)^2+\left(\frac{\partial\tilde{u}_\theta}{\partial z}\right)^2+\left[r\frac{\partial}{\partial r}\left(\frac{\tilde{u}_\theta}{r}\right)\right]^2-\frac{2}{3}\left(\nabla\cdot\widetilde{\vec{V}}\right)^2\right\}$

Note: $\mu_{\mathrm{eff}}=\mu_{\mathrm{lam}}+\mu_{\mathrm{turb}}$, $\left(\frac{\mu}{Pr}\right)_{\mathrm{eff}}=\left(\frac{\mu_{\mathrm{lam}}}{Pr}\right)+\left(\frac{\mu_{\mathrm{turb}}}{Pr_T}\right)$, $h=C_PT$, $\widehat{P}=\widetilde{P}+\frac{2}{3}\bar{\rho}E_{\mathrm{SGS}}$, $E_{\mathrm{SGS}}=\frac{\nu_T^2}{(C_I\overline{\Delta})^2}$, $C_I=0.094$, $Pr_T=0.9$, $\nu_T=\frac{\mu_{\mathrm{turb}}}{\bar{\rho}}$.

BTDC during isentropic process. The wall temperature is assumed to be 320 K, and thereby simulating the case of a cold engine state. The wall function [19] is used to provide wall boundary conditions for velocity and temperature in the near-wall region.

In the laminar sublayer,

$$U^+ = Y^+ \tag{7}$$

$$T^+ = Pr\,Y^+ - 0.5Pr\,S^+\left(Y^+\right)^2 \tag{8}$$

$$Y^+ < 13.2$$

In the turbulent boundary layer,

$$U^+ = \frac{1}{\kappa}\ln EY^+ \tag{9}$$

$$T^+ = 13.2Pr + 2.195\ln Y^+ - 5.66 - S^+\left(87.12Pr + 2.195Y^+ - 28.98\right) \tag{10}$$

$$Y^+ \geqslant 13.2$$

Dimensionless variables with a superscript plus sign are defined as follows:

$$Y^+ \equiv \frac{yU^*}{\nu}, \qquad U^+ \equiv \frac{\widetilde{U}}{U^*}$$

$$T^+ \equiv \frac{\bar{\rho}C_P(\widetilde{T} - T_W)U^*}{q_w}, \qquad S^+ \equiv \frac{S\nu}{q_w U^*} \tag{11}$$

The friction velocity U^* is defined as

$$U^* \equiv \sqrt{\frac{\tau_w}{\bar{\rho}}} \tag{12}$$

where ν is laminar kinematic viscosity, Pr is the Prandtl number, y is the distance from the wall, $\widetilde{U}$ denotes the velocity component parallel to the wall, and S is the modified factor of the temperature boundary layer model as defined in Huh et al. study [19]. When $S = 0$, the model corresponds to the original logarithmic law of the wall.

The calculations are started at a crank angle of 240° (120° BTDC) in the compression stroke and terminated at 400° (40° ATDC) in the expansion stroke for an engine speed of 900 rpm. The initial air condition is set to be a solid-body rotation profile, $\tilde{u}_\theta(r) = 2\pi r N_{\text{rpm}} SR_o/60$, where N_{rpm} is the engine speed and SR_o (called the initial swirl ratio) is defined as the ratio of initial swirling speed (rpm) of the gas to engine speed. The axial velocity $\tilde{u}_z$ is assumed to vary linearly from cylinder head surface (zero velocity) to piston crown surface (moving boundary velocity). The radial velocity $\tilde{u}_r$ is assumed to be zero. The initial temperature is set equal to be 320 K. The engine used for computation is a four-stroke engine with various bowl model pistons.

3. Numerical method

The numerical method for presenting the discretized transport equations is based on the SIMPLE-C algorithm using the control volume approach with each equation arranged into transient, diffusion, convection, and source terms. In addition, the second-order backward Euler (SBE) method [8] for discretizing the transient term and the Extended Linear Upwind Differencing (ELUD) method [9] for discretizing the convective term are adopted in the SIMPLE-C Navier–Stokes algorithm.

The iterative solution methods based on the pre-conditioned conjugate gradient methods [10,11] are incorporated into this calculation to solve the transport equations. Three crank angle steps 0.5°, 1°, and 2° are used to test the independence of crank angle step. According to the sensitivity results, the crank angle step was set as 1° for the calculations of transient flow and heat transfer in the combustion chamber; we consider the difference in the calculated variables $\widetilde{\Phi}$ and the mass residual (M_P) of pressure-correction equation as convergence conditions for each grid point. The following criterion was used for the computation:

$$M_P = b^n = a_P \widetilde{P'}_P^n - \sum a_{\text{nb}} \widetilde{P'}_{\text{nb}}^n < 10^{-4} \tag{13}$$

$$\frac{|\widetilde{\Phi}_P^{n+1} - \widetilde{\Phi}_P^n|}{\max|\widetilde{\Phi}_P^{n+1}|} < 10^{-5} \tag{14}$$

where n is the iteration number, a_{nb} is neighbor coefficient at the control-volume faces, P' is pressure correction and b represents the mass source in the pressure-correction equation [20].

The grid generation approach is used to treat the moving piston as a moving solid body in the computational domain without generating completely new grids at each crank angle step. When the piston moves toward TDC or from TDC, the size of the domain will vary with the motion of the piston and those grids lying outside the body will be flagged as unused points that are excluded from the calculation. If the cell attached to the piston face was smaller than half of the size of the previous fixed grid cell, then it was merged with the previous grid cell; otherwise, a smaller grid cell was attached to the piston face. When the piston was moving away from TDC, it was necessary not only to interpolate the values back to their fixed grid locations but also to extrapolate the values of the time dependent variables for two grid cells into the piston. This extrapolation was performed with a second-order Lagrange polynomial. To minimize the errors due to the interpolations or extrapolations, the piston was allowed to move no more than one grid spacing (in the axial direction) per crank angle step.

4. Results and discussion

Numerical calculations of the in-cylinder thermal flow field have been performed systematically to investigate the influence of compression ratio CR and initial swirl ratio SR_o on the transient turbulent heat transfer in the motored engine. In this study, the engine parameters are taken as 900 rpm (speed), 83.0 mm (bore) and 85.0 mm (stroke) with various compression ratios (CR is equal to 6.8, 8.7, and

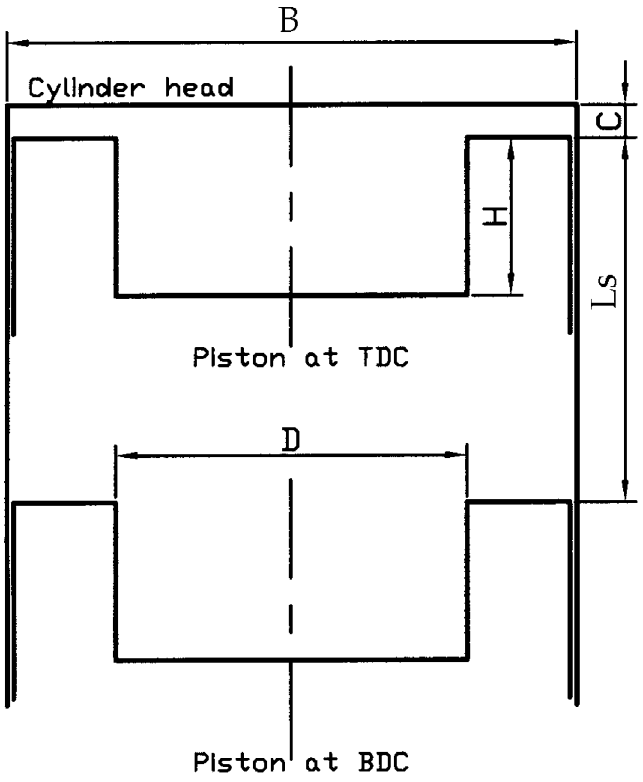

B	D	H	Ls	C	*CR*
0.083 m	0.04 m	0.0225 m	0.085 m	0.0093 m	6.8
				0.0057 m	8.7
				0.0036 m	10.6

Intake valve opens at 16.5° BTDC; Intake valve closes at 48.5° ABDC. Exhaust valve opens at 48° BBDC; Exhaust valve closes at 12° ATDC [4].

Fig. 1. Combustion chamber geometry for the bowl piston engine.

10.6) and different initial swirl ratios (SR_o is set equal to be 1.325, 5.3, and 9.5). The above parameters are selected according to the study presented by Kondoh et al. [4]. The bowl-in-piston combustion chamber is considered as Fig. 1 shows. All the calculations have been performed by using a PENTIUM II 300 PC. After testing the three meshes (mesh I: 126 × 250 for 240° (120° BTDC) ∼ grid 126 × 94 for 360° (TDC) ∼ grid 126 × 112 for 400° (40° ATDC); mesh II: grid 105 × 207 for 240° (120° BTDC) ∼ grid 105 × 78 for 360° (TDC) ∼ grid 105 × 93 for 400° (40° ATDC); mesh III: grid 84 × 166 for 240° (120° BTDC) ∼ grid 84 × 63 for 360° (TDC) ∼ grid 84 × 75 for 400° (40° ATDC)), the mesh II was chosen for all cases on the basis of 1.5–3.4% error sensitivity. The calculation for this study utilized 480 crank angle steps and the computation time was about 4 and half hours of CPU time.

For the purpose of showing that the program in this study correctly handles the turbulent thermal flow field in a motored engine, we apply the present method to solve the transient heat transfer in a motored engine with a flat piston crown employed by Yang et al. [21]. The engine parameters used by them and us include bore (91.9 mm), stroke (76.2 mm), compression ratio ($CR = 9.5$) and initial

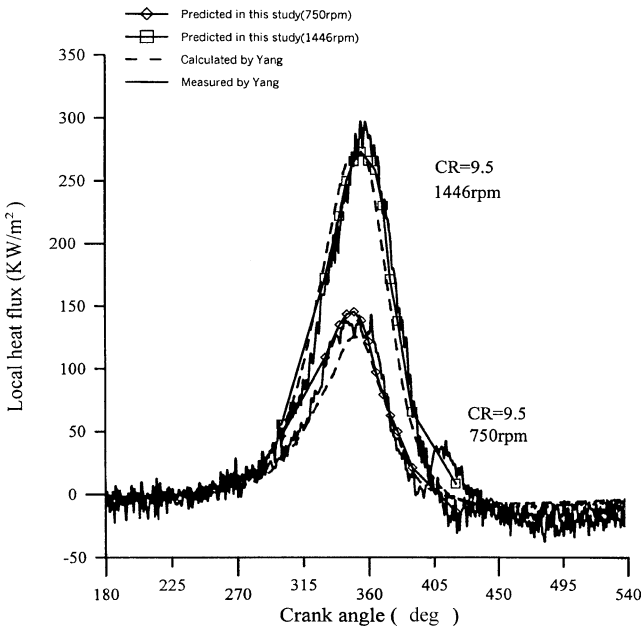

Fig. 2. Comparison of predicted local wall heat flux on cylinder head surface with experimental data and calculated results of Yang ($r = 20.0$ mm).

swirl ratio ($SR_o = 0.5$) while the engine speed is 750 rpm and 1446 rpm. The predicted transient heat flux on head surface presented in Fig. 2 agrees well with the experimental data and calculated results of Yang et al.

The combined velocity vectors of $\tilde{u}_r$ and $\tilde{u}_z$ at 300° (60° BTDC), 330° (30° BTDC), 350° (10° BTDC), 360° (TDC), and 370° (10° ATDC) are presented in Fig. 3 to investigate the flow field in the combustion chamber. At 300°, an increase in upward piston speed causes radial velocity vectors smaller than axial ones near the piston crown (Fig. 3(a)). When the piston continues to compress upward until 330°, the instantaneous piston speed is weaker and the squish effect is going to develop after the fluids are brought from the periphery into the piston bowl (Fig. 3(b)). In other words, there is strong radial flow toward the axis (called "squish motion") above the piston head, which is caused by the large difference of compression between the inner (smaller radius) and the outer (bigger radius) region. Moreover, the squish motion interacting with higher swirl velocity forms the vortex in the bowl. At 350°, the stronger squish effect with weaker piston speed produces a vortex with the clockwise rotation in the bowl (Fig. 3(c)). When the squish motion almost terminates at TDC, there is another vortex with the counter-clockwise rotation around the top of the piston bowl (Fig. 3(d)). After the piston passes through TDC, owing to downward piston motion, the fluids are sucked up into the periphery, and the appearance forms the "reversing squish motion" (Fig. 3(e)). These results provide confirmation to flow processes in the bowl-in-piston combustion chamber of a motored engine.

Fig. 4 shows the contour lines of swirl velocity $\tilde{u}_\theta$ in the combustion chamber at various crank angles. The distribution of $\tilde{u}_\theta$ does not differ so much from that of the

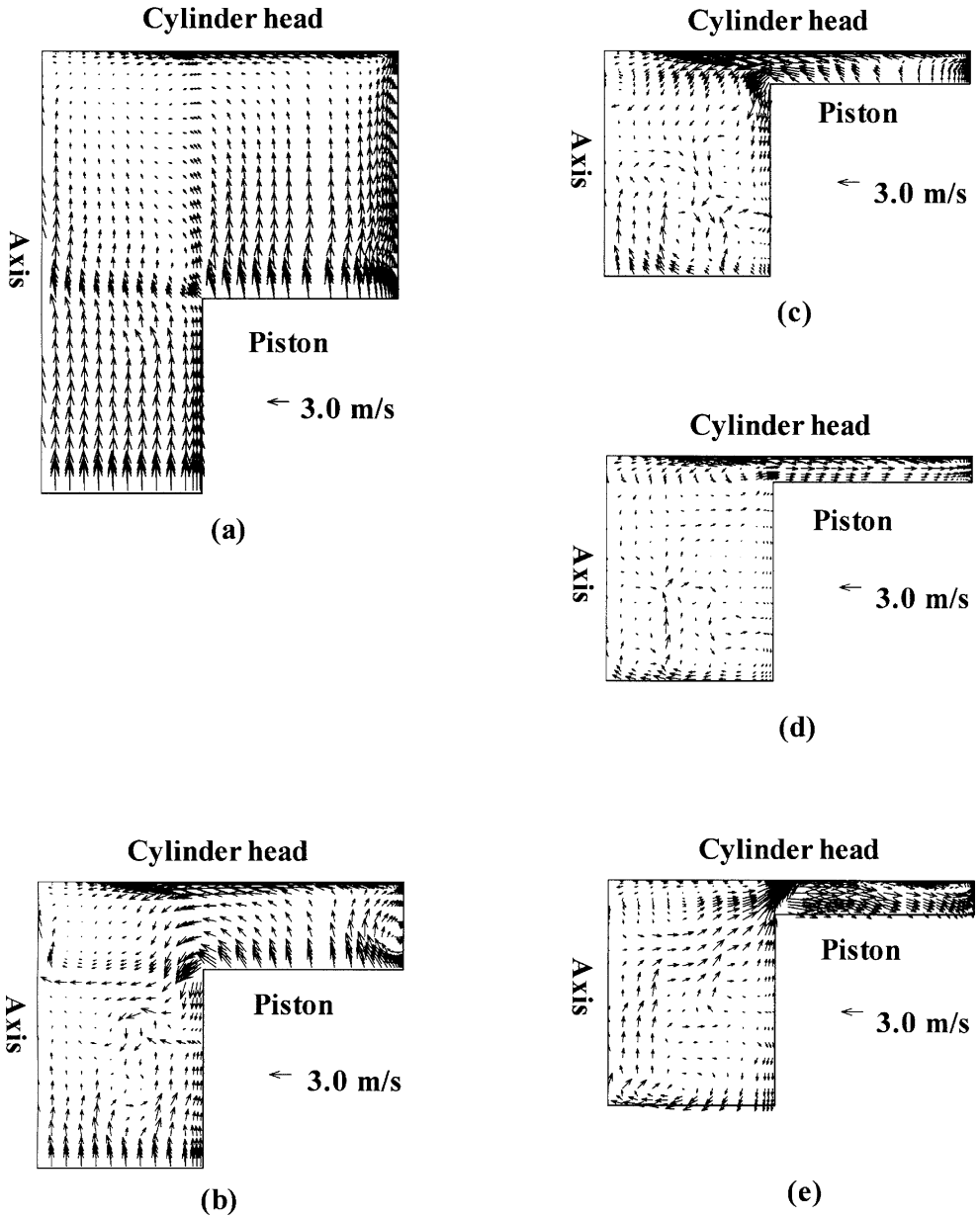

Fig. 3. The combined velocity vectors of $\tilde{u}_r$ and $\tilde{u}_z$ for $CR = 10.6$ and $SR_o = 5.3$ in the combustion chamber at θ equal to (a) 300°; (b) 330°; (c) 350°; (d) TDC; (e) 370°, and only one of every three grid points is shown for clarity.

initial swirl profile until crank angle reaches about 300°. After that crank angle, as the angular momentum in the squish region is transferred into the piston bowl by the squish flow (see Fig. 4(b)), the position of the maximum value of $\tilde{u}_\theta$ moves into the piston bowl at 350° (see Fig. 4(c)). $\tilde{u}_\theta$ at TDC almost has the same distribution as that at 350° in the piston bowl. After TDC, the maximum value of $\tilde{u}_\theta$ decreases, but it occurs near the top edge of the piston bowl.

For realizing the heat transfer characteristics, this study checks over the mean surface heat flux for the cylinder head, the cylinder wall and the piston crown. The mean surface heat flux on the surface is presented in Fig. 5 for different parts of combustion chamber and different crank angles, ranging from 300° (60° BTDC) to 390° (30° BTDC), at $CR = 10.6$ and $SR_o = 5.3$ under 900 rpm. For cylinder head surface, the peak value occurs at 350° (10° BTDC); 355° (5° BTDC) for piston crown surface (1) and (2); 360° (TDC) for piston crown surface (3) and cylinder wall surface. Besides, it may be noted that the surface heat fluxes near 5° BTDC are much higher for cylinder head surface and piston crown surface (1) than for the cylinder wall and the other two piston crown surfaces. This behavior implies that there is an obvious squish effect on cylinder head surface and piston crown surface (1) from crank angles 350° to 360°. At 300°, the mean surface heat fluxes on all surfaces are small because the radial velocity vectors are smaller than axial ones near the piston crown. When the squish effect is developing about 330°, the squish motion interacting with

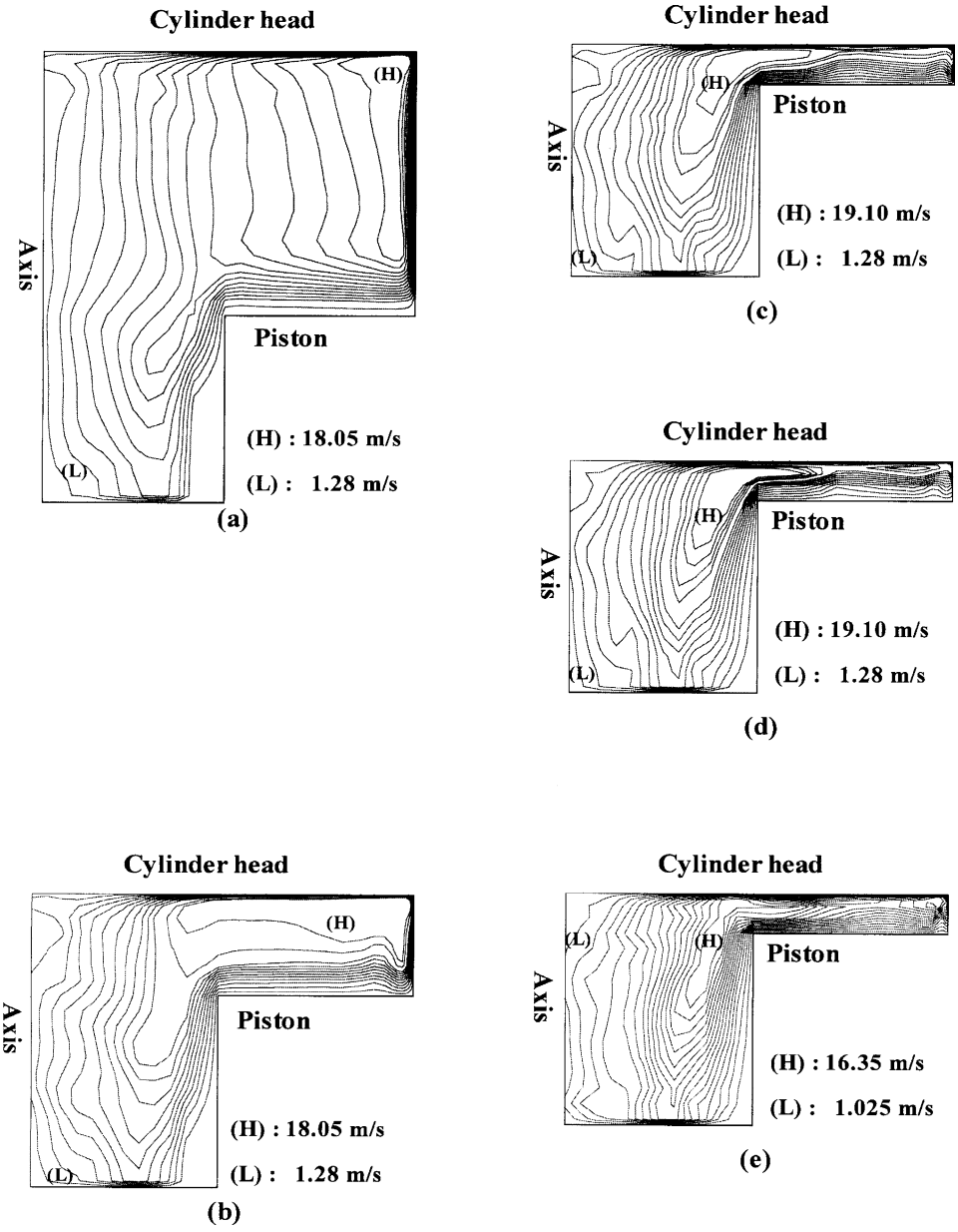

Fig. 4. The contour lines of swirl velocity $\tilde{u}_\theta$ for $CR = 10.6$ and $SR_o = 5.3$ in the combustion chamber at θ equal to (a) 300°; (b) 330°; (c) 350°; (d) TDC; (e) 370°.

higher swirl velocity makes the mean surface heat flux get higher for cylinder head than for the other parts. At 350°, the stronger squish effect with weaker piston speed strengthens the mean surface heat flux much more for cylinder head surface and piston crown surface (1) than for the other parts. At TDC, the higher two heat fluxes reduce suddenly because the squish motion almost terminates. About 390°, the heat fluxes reach to the minimum value and tend to be negative; that is, the heat is going to transfer from walls to the fluids. According to the results from Figs. 3–5, we find that squish effect not only strengthens the wall heat transfer but also enhances swirl velocity. Stronger swirl means more rapid mixing of fluid in diesel or stratified charge engines, or promoting a fast burn in spark ignition engines.

The compression ratio CR plays an important role for affecting the internal flow of an engine, so we investigate the fluid flow and contour lines of $\tilde{u}_\theta$ at 350° and $SR_o = 5.3$ for various compression ratios (CR is taken as 6.8, 8.7, and 10.6) in the combustion chamber as shown in Figs. 6 and 7. In Fig. 6, the clearance volume at $CR = 6.8$ is bigger than that at $CR = 8.7$ and $CR = 10.6$; hence, a small amount of fluid is brought from the periphery into the piston bowl at $CR = 6.8$ in the combustion chamber. On the contrary, the higher value of compression ratio results in stronger radial velocity around the top edge of the piston bowl and the vortex in the bowl as shown in Fig. 6. In other words, the squish effect at $CR = 10.6$ is the strongest among the three cases in Fig. 6. For realizing the influence

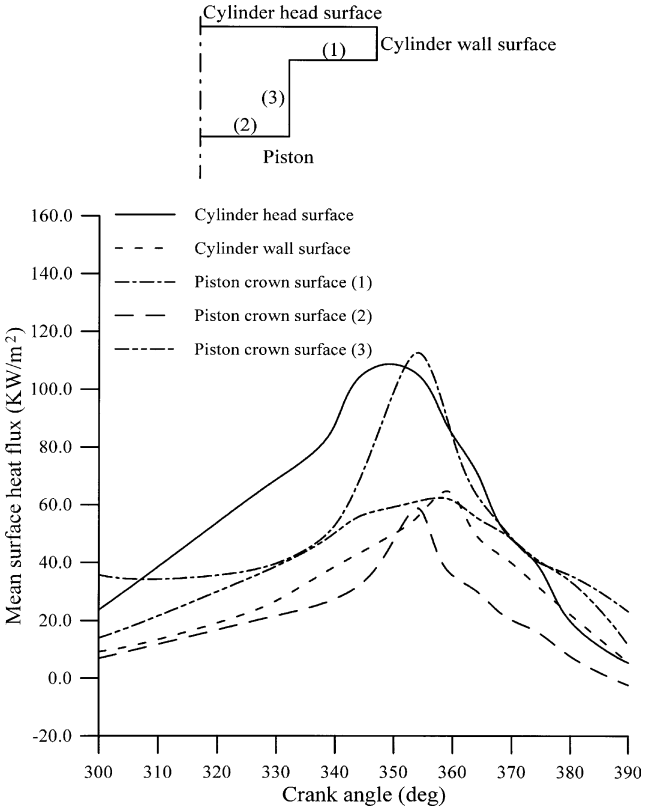

Fig. 5. Transient mean surface heat flux on different surfaces for various crank angles at $CR = 10.6$ and $SR_o = 5.3$ in the combustion chamber.

of compression ratio on the swirl flow in the combustion chamber, we observe the contour lines of $\tilde{u}_\theta$ as shown in Fig. 7. The maximum value of $\tilde{u}_\theta$ near the top edge of the piston bowl increases and this contour line moves more into the piston bowl with an increase in CR (see Fig. 7). According to these results of Figs. 6 and 7, we find that higher compression ratio CR obviously gets stronger squish effect in the combustion chamber. For realizing the effect of compression ratio on the squish motion, we observe the time histories of $\Omega^* = \Omega/\Omega_o$ and SR_m in the combustion chamber with various values of compression ratio (CR is taken as 6.8, 8.7, and 10.6) when the initial swirl ratio SR_o is kept constant at 5.3 and the engine speed is 900 rpm shown in Fig. 8. Fig. 8(a) reveals that the decay rate of Ω^* is almost the same for various values of CR before 340° (20° BTDC) while it increases with increasing the value of CR after 340°. As shown in Fig. 8(b), there is almost no difference in the value of SR_m between three values of CR before 310° (50° BTDC) but the value of SR_m becomes higher with increasing the value of CR after 310°. Furthermore, the difference is the most obvious between 350° (10° BTDC) and 360° (TDC) for $CR = 10.6$; this indicates a higher value of compression ratio would enhance the swirl strength especially as the piston approaches TDC. The value of SR_m is found to be related to the decay rate of Ω^* and the maximum value of SR_m occurs at the maximum decay rate of Ω^*. The above differences for the values

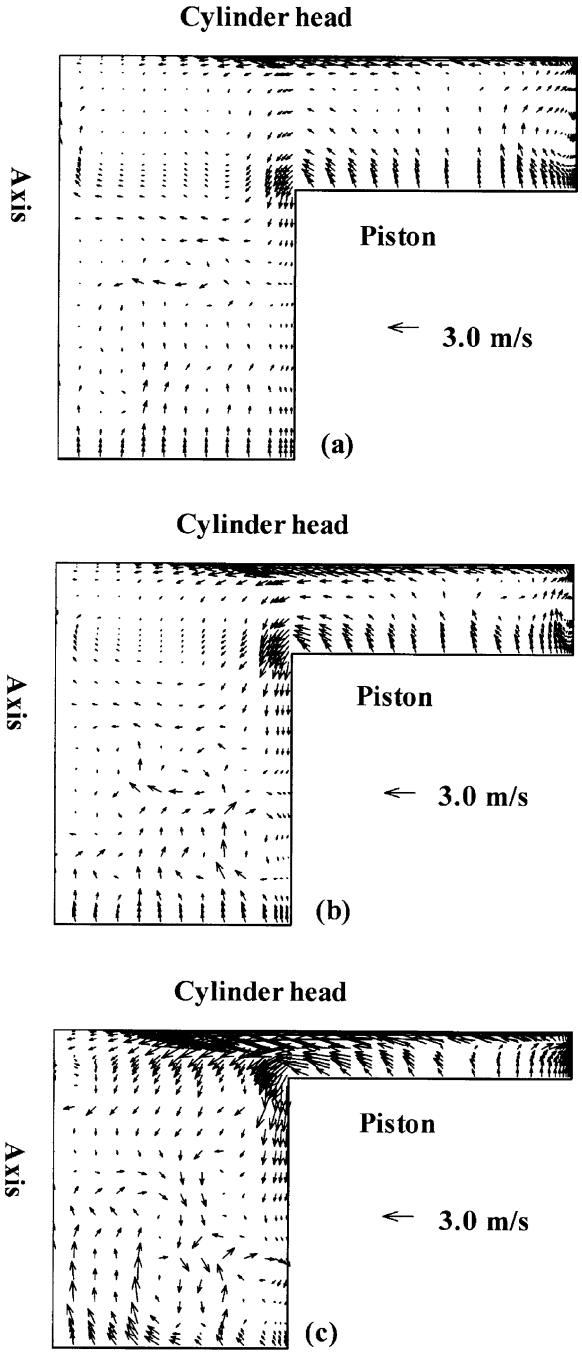

Fig. 6. The combined velocity vectors of $\tilde{u}_r$ and $\tilde{u}_z$ at crank angle 350° for (a) $CR = 6.8$; (b) $CR = 8.7$; (c) $CR = 10.6$ and $SR_o = 5.3$ in the combustion chamber, and only one of every three grid points is shown for clarity.

of Ω^* and SR_m between three values of CR are caused by various strengths of the squish motion. An increase in the decay rate of Ω^* with increasing a value of CR is explained from the fact that more fluid momentum in the squish region is transferred into the bowl. Besides, a faster decay rate of normalized angular momentum represents that the maximum value of swirl velocity is transferred into the bowl, which is effective in more rapid mixing of fluid in

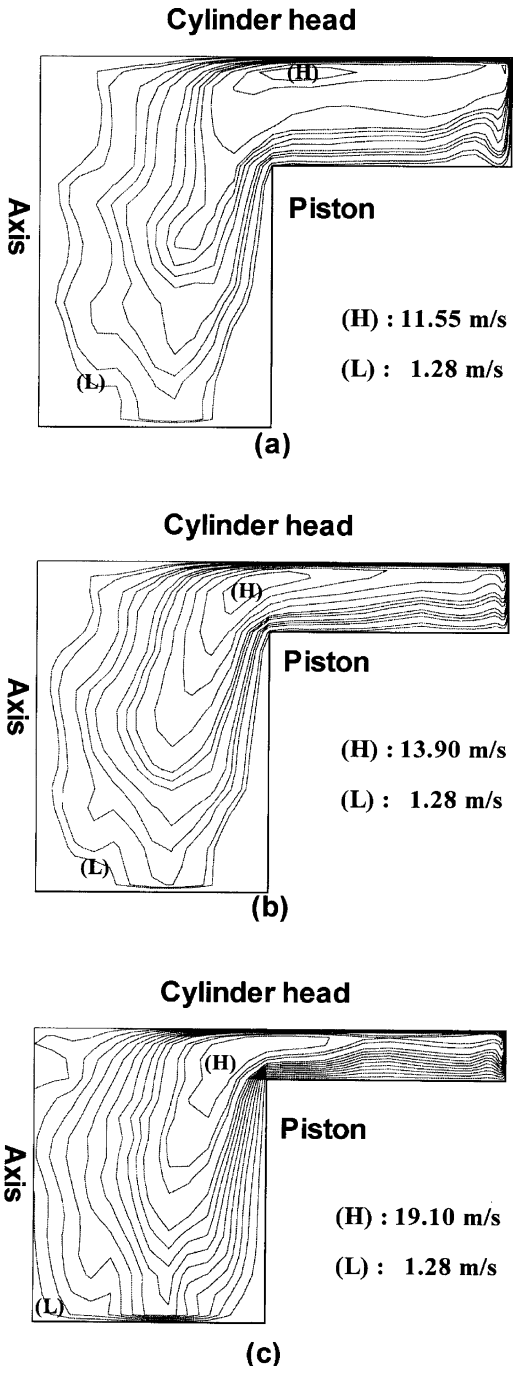

Fig. 7. The contour lines of swirl velocity $\tilde{u}_\theta$ at crank angle 350° for (a) $CR = 6.8$; (b) $CR = 8.7$; (c) $CR = 10.6$ and $SR_o = 5.3$ in the combustion chamber.

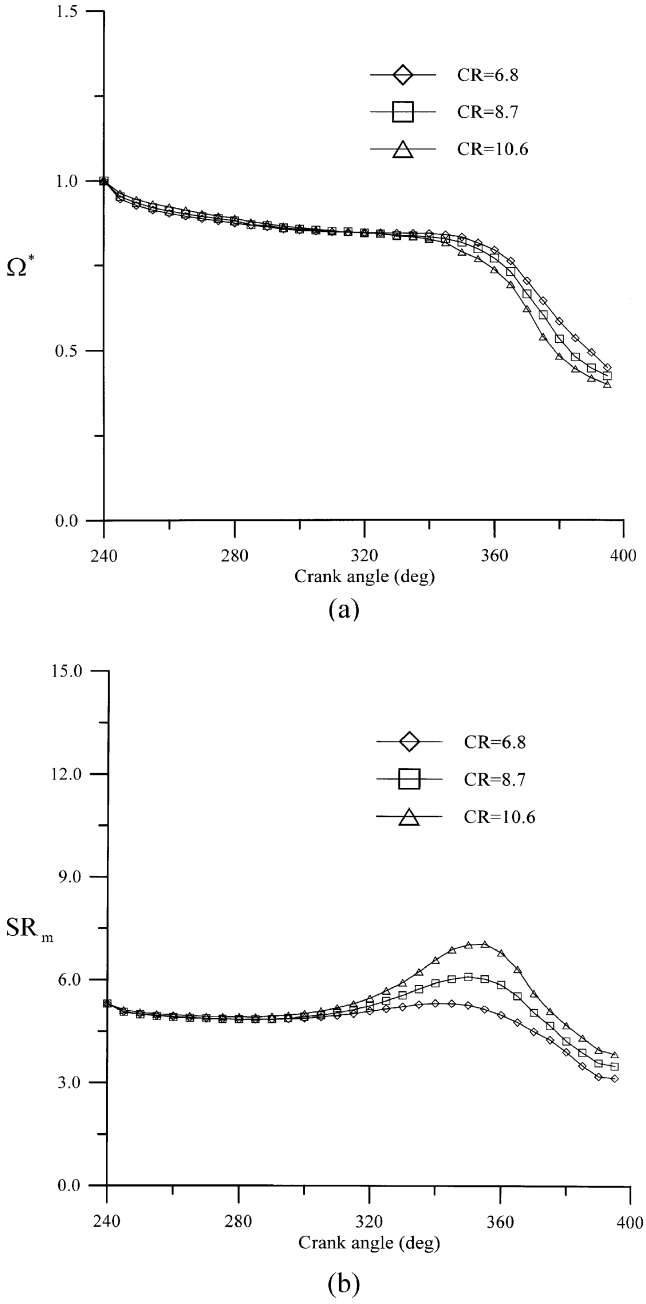

Fig. 8. Effects of compression ratio on (a) Ω^*; (b) SR_m at $SR_o = 5.3$ in the combustion chamber under an engine speed of 900 rpm.

diesel or stratified charge engines, or promoting a fast burn in spark ignition engines.

Fig. 9 shows that the mean surface heat flux on all surfaces at $SR_o = 5.3$ for various CR values in the combustion chamber. Increasing compression ratio CR makes the piston do more work on the air in the combustion chamber during the compression stroke; hence, the temperature and pressure of air are becoming higher. Due to these reasons, the profile of mean surface heat flux is increasing as CR increases. The increase in the time-average value of the mean surface heat flux is about 39% when CR is ranged from 6.8 to 10.6. During the expansion stroke, the air in the combustion chamber does more work on the piston with increasing CR. The result makes the profile of mean surface heat flux after 23° ATDC decrease. Besides, the proportion of increase in the mean surface heat fluxes between 350° (10° BTDC) and 360° (TDC) is obviously bigger than the increase in CR value due to the enhancement of squish effect by a higher compression ratio. Fig. 10 illustrates the isothermal distribution at 350° and $SR_o = 5.3$ for various CR val-

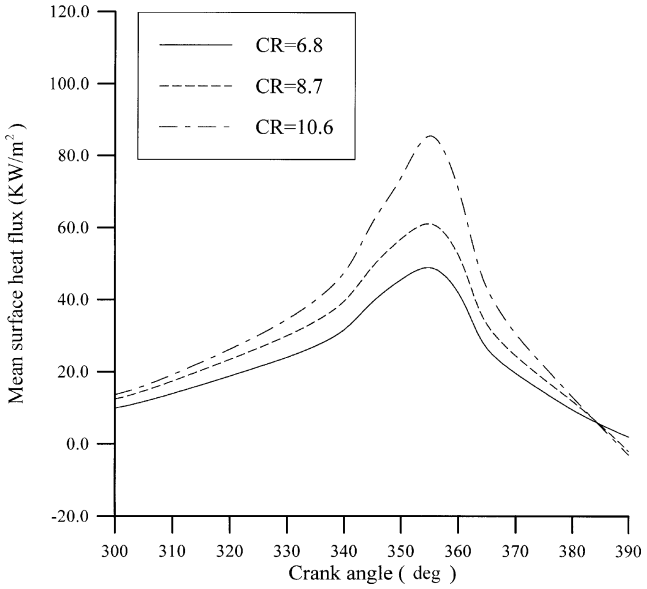

Fig. 9. Transient mean surface heat flux on all surfaces at $SR_o = 5.3$ for various CR values in the combustion chamber.

ues. Closer isothermal lines indicate higher temperature gradients and accordingly higher heat fluxes. The temperature of air in the combustion chamber is increasing with increasing CR, so the temperature gradient along the surface becomes higher.

Due to the importance of swirl flow in the combustion chamber, we observe the fluid flow and contour lines of $\tilde{u}_\theta$ at 350° for various initial swirl ratios (SR_o is taken as 1.325, 5.3, and 9.5) as shown in Figs. 11 and 12. In Fig. 11, the combined velocity vectors of $\tilde{u}_r$ and $\tilde{u}_z$ along the surface of cylinder head become stronger with an increase in the initial swirl ratio SR_o. Furthermore, the vortex in the bowl becomes stronger and is closer to the bottom of piston bowl with increasing SR_o. The profiles of $\tilde{u}_\theta$ as shown in Fig. 12 present that the maximum value of $\tilde{u}_\theta$ around the top edge of piston bowl increases with an increase in SR_o. These results shown in Figs. 11 and 12 reveal that higher initial swirl ratio SR_o leads to stronger squish effect on the fluid flow. For comprehending the influence of initial swirl ratio on the flow field and mixing of fluid, we investigate the variations of Ω and SR_m at different crank angles. Shown in Fig. 13 are the variations of the ratio $\Omega^* = \Omega/\Omega_o$ and SR_m with various crank angles in the combustion chamber with various values of initial swirl ratio (SR_o is taken as 1.325, 5.3 and 9.5) under the conditions that the compression ratio CR is kept constant at 10.6 and the engine speed is 900 rpm. In Fig. 13(a), we find that the decay rate of Ω^* becomes large with an increase in SR_o (similar tendency as found in the results of Kuo and Duggal [22]). This is due to a larger value of diffusivity for the same diffusive time. Then, the value of SR_m increases, and shifts from TDC to 15 deg BTDC with increasing SR_o as shown in Fig. 13(b).

Fig. 14 shows that the mean surface fluxes on all surfaces of combustion chamber at $CR = 10.6$ for different initial

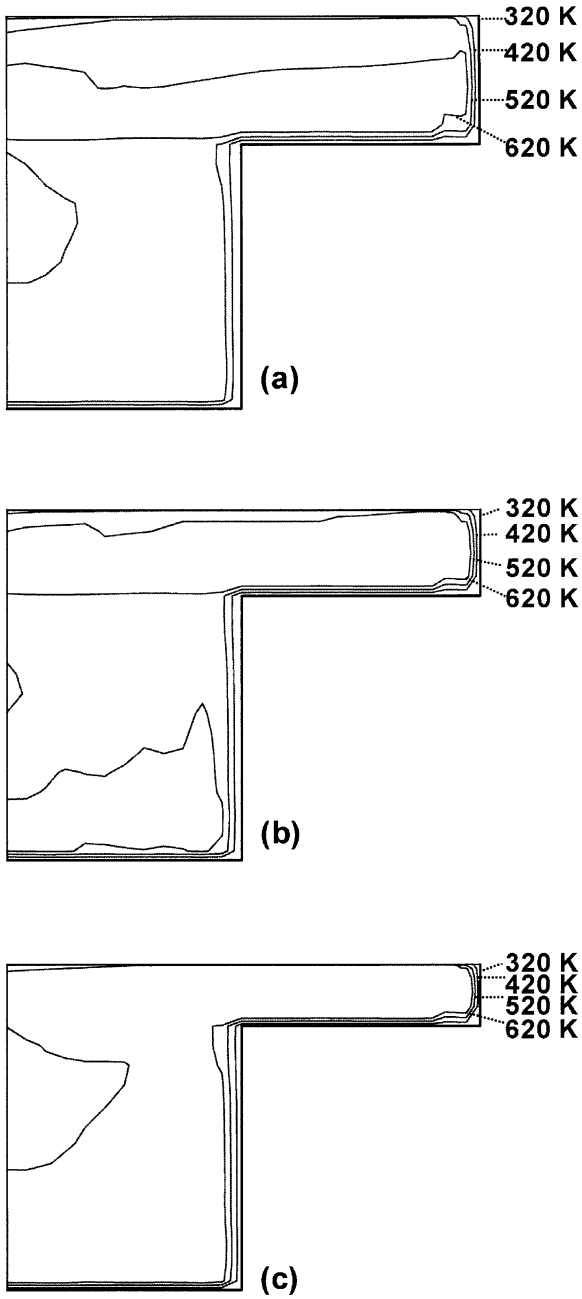

Fig. 10. Isotherms at $\theta = 350°$ and $SR_o = 5.3$ in the combustion chamber for (a) $CR = 6.8$; (b) $CR = 8.7$; (c) $CR = 10.6$.

swirl ratio SR_o values. With increasing SR_o, the mean surface heat fluxes increase because the fluid flow velocity and turbulent kinetic energy become stronger. The increase in the time-average value of mean surface heat flux along all surfaces of the combustion chamber is about 67% when SR_o is ranged from 1.325 to 9.5 Besides, the peak heat flux is shifting to 7° BTDC from 3° BTDC with increasing initial swirl ratio SR_o The phase shift occurs due to the competing effects of the gas temperature which peaks at TDC and the rate-of-pressure rise term which peaks around 90° BTDC at the maximum piston speed and compression rate. About 390°, the mean surface heat fluxes are negative

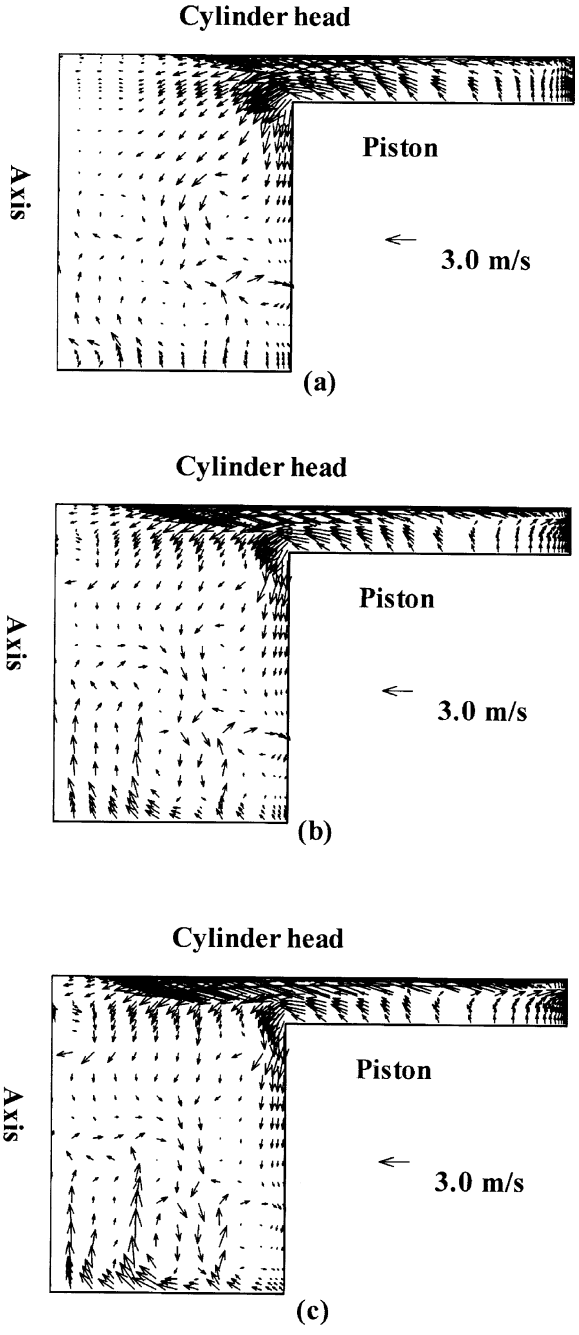

Fig. 11. The combined velocity vectors of $\tilde{u}_r$ and $\tilde{u}_z$ at crank angle 350° and $CR = 10.6$ or (a) $SR_o = 1.325$; (b) $SR_o = 5.3$; (c) $SR_o = 9.5$ in the combustion chamber, and only one of every three grid points is shown for clarity.

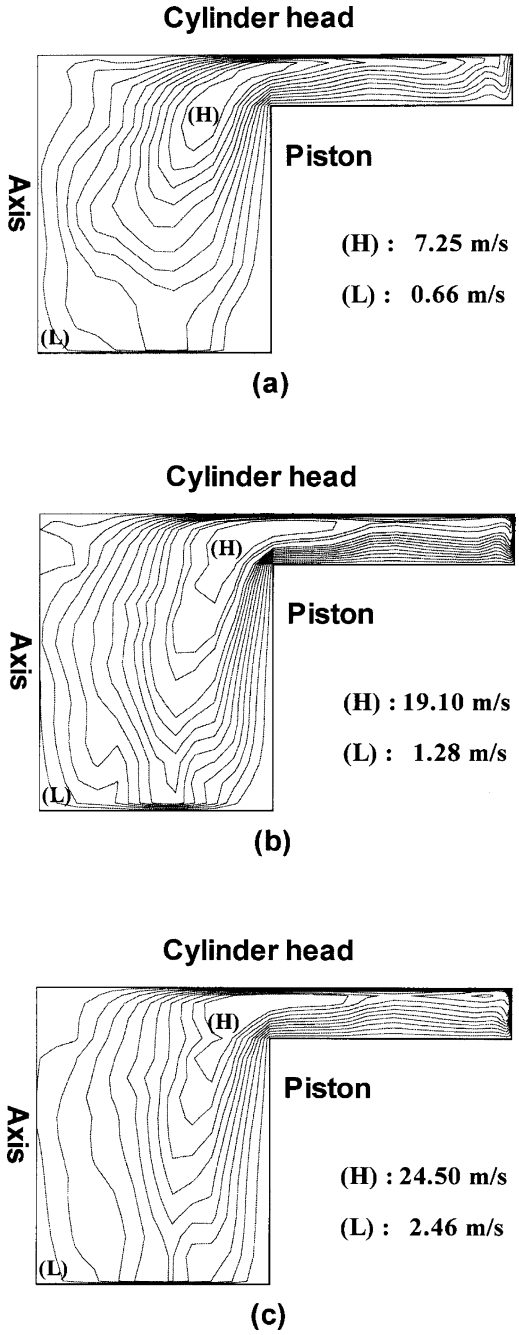

Fig. 12. The contour lines of swirl velocity $\tilde{u}_\theta$ at crank angle 350° and $CR = 10.6$ for (a) $SR_o = 1.325$; (b) $SR_o = 5.3$; (c) $SR_o = 9.5$ in the combustion chamber.

at $SR_o = 5.3$ and 9.5 resulting from stronger reversing squish motion. Fig. 15 illustrates the isothermal distribution at 350° and $CR = 10.6$ for various initial swirl ratio SR_o values. All fluid motion becomes stronger as SR_o increases. This increases the temperature gradient along the surfaces of each part in the combustion chamber, especially along the surfaces influenced by squish motion. Besides, the local high temperature in the bowl increases with an increase in SR_o.

5. Conclusions

A numerical method was applied to the transient turbulent thermal flow during the compression-expansion strokes in the combustion chamber when an engine operates at various compression ratio CR and initial swirl ratio SR_o values. It is expected that the numerical method can be successfully used in the practical problems to understand the phenomena occurring in the engine and to obtain the design parameters.

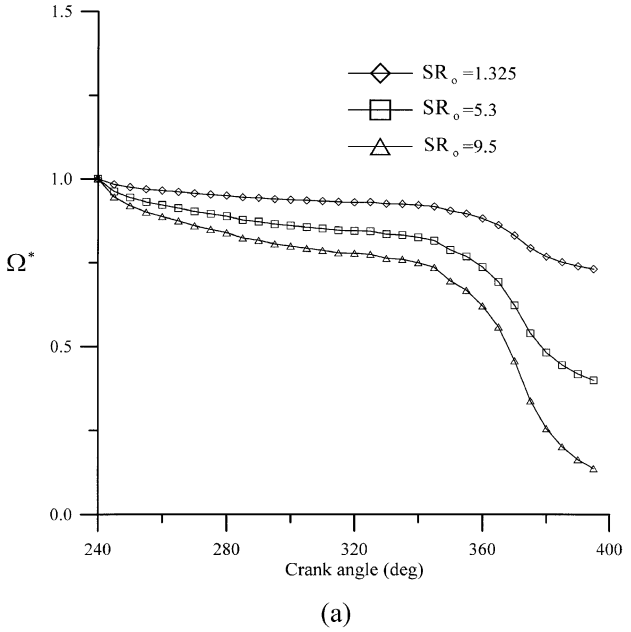

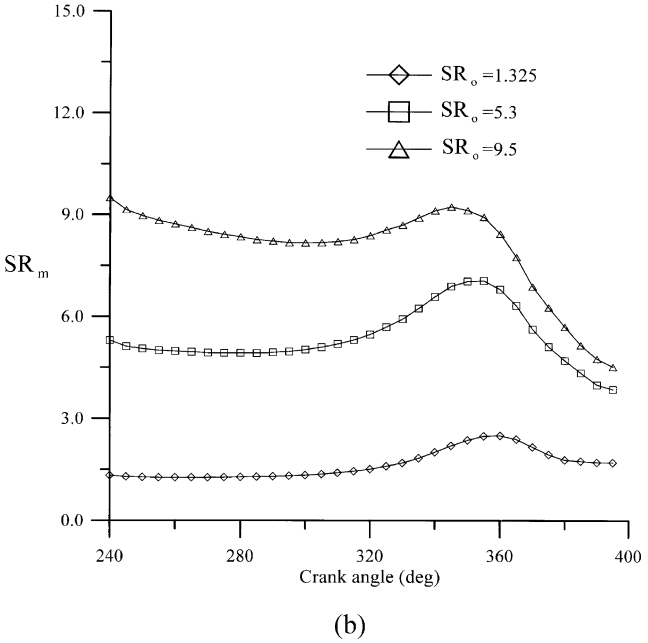

Fig. 13. Effects of initial swirl ratio on (a) Ω^*; (b) SR_m at $CR = 10.6$ in the combustion chamber under an engine speed of 900 rpm.

On the basis of these results presented and discussed in the discussion section, we draw the main conclusions below:

(1) After a comparison with the previous researcher's results, large Eddy simulation which was implemented into the SIMPLE-C algorithm coupled with pre-conditioned conjugate gradient methods can predict the turbulent heat transfer in the combustion chamber of a motored engine with reasonable accuracy.
(2) The surface heat fluxes near 5° BTDC are much higher for cylinder head surface and piston crown surface except for the bowl of piston than for the cylinder wall

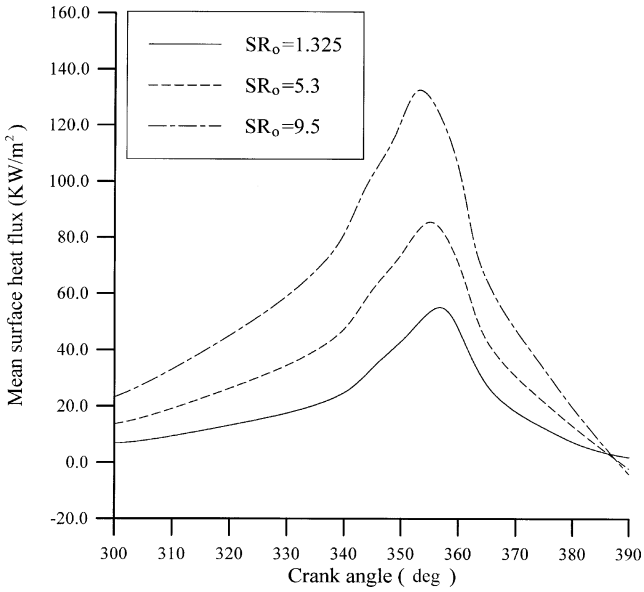

Fig. 14. Transient mean surface heat flux on all surfaces at $CR = 10.6$ for various SR_o values in the combustion chamber.

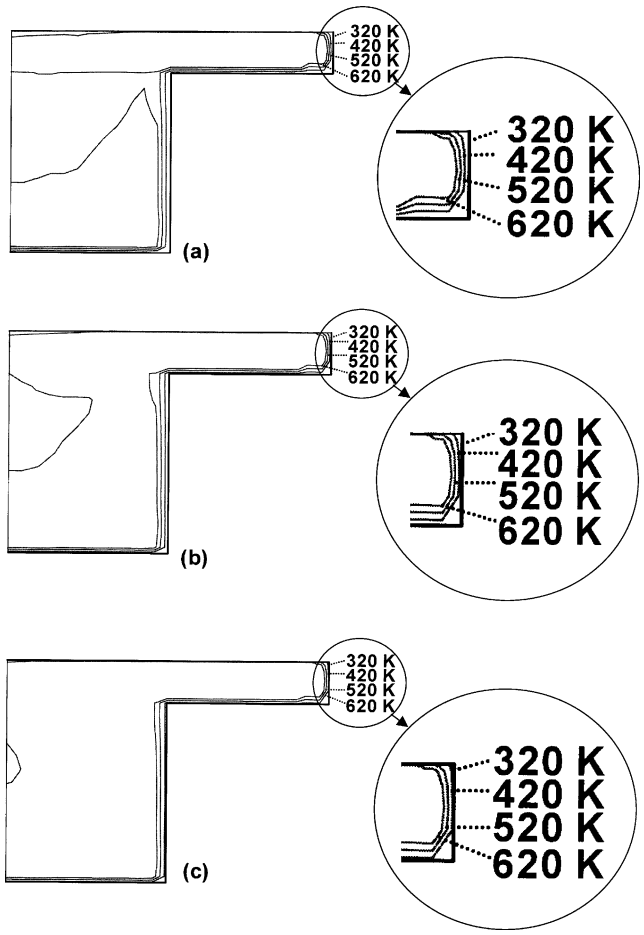

Fig. 15. Isotherms at $\theta = 350°$ and $CR = 10.6$ in the combustion chamber for (a) $SR_o = 1.325$; (b) $SR_o = 5.3$; (c) $SR_o = 9.5$.

and the piston bowl surfaces. Besides, the peak heat flux is shifting to 7° BTDC from 3° BTDC with increasing initial swirl ratio SR_o.

(3) With increasing the compression ratio or the initial swirl ratio, the vortex produced from the squish flow and the swirl become stronger in the bowl due to an increase in the decay rate of normalized angular momentum. Stronger swirl means more rapid mixing of fluid in diesel or stratified charge engines, or promoting a fast burn in spark ignition engines.

(4) The increase in the time-average value of mean surface heat flux along all surfaces of the combustion chamber is about 67% when SR_o is ranged from 1.325 to 9.5; the increase in the time-average value of the mean surface heat flux is about 39% when CR is ranged from 6.8 to 10.6.

(5) Interaction between piston motion, induced squish and swirl motion has great influences in determining the transient thermal flow fields, so obtaining such information is useful for designing engines.

Acknowledgement

The authors gratefully acknowledge the partially financial support of this project by the National Science Council of the Republic of China.

References

[1] D.N. Assanis, E. Badillo, Evaluation of alternative thermocouple designs for transient heat transfer measurements in metal and ceramic engines, SAE Paper 890571, 1989.

[2] K. Dao, O.A. Uyehara, P.S. Myers, Heat transfer rates at gas-wall interfaces in motored piston engine, SAE Paper 730632, 1973.

[3] T. Morel, S. Wahiduzzaman, D.R. Tree, D.P. Dewitt, Effect of speed, load, and location on heat transfer in a diesel engine—measurement and predictions, SAE Paper 870154, 1987.

[4] T. Kondoh, A. Fukumoto, K. Ohsawa, Y. Ohkubo, An assessment of a multi-dimensional numerical method to predict the flow in internal combustion engines, SAE Paper 850500, 1986.

[5] M. Ikegami, Y. Kidoguchi, K. Nishiwaki, A multidimensional prediction of heat transfer in non-fired engines, SAE Paper 860467, 1986.

[6] G. Raithby, I. Van Doormaal, Enhancements of the SIMPLE method for predicting incompressible fluid flows, Numer. Heat Transfer 7 (1984) 147–163.

[7] B. Galperin, S. Orszag, Large Eddy Simulation of Complex Engineering and Geophysical Flows, first ed., Cambridge University Press, Cambridge, 1993, p. 231.

[8] G.B. Deng, J. Piquet, P. Queutey, M. Visonneau, A new fully coupled solution of the Navier–Stokes equations, Internat. J. Numer. Methods Fluids 19 (1994) 605–639.

[9] Y.Y. Tsui, A study of upstream weighted high-order differencing for approximation to flow convection, Internat. J. Numer. Methods Fluids 13 (1991) 167–199.

[10] D. Kershaw, The incomplete Cholesky-conjugate gradient method for the iterative solution of systems of linear equations, J. Comput. Phys. 26 (1978) 43–65.

[11] H. Van Der Vorst, BI-CGSTAB: A fast and smoothly converging variant of BI-CG for the solution of non-symmetric linear system, SIAM J. Sci. Statist. Comput. 13 (2) (1992) 631–644.

[12] J.Y. Tu, L. Fuchs, Overlapping grids and multi-grid methods for three-dimensional unsteady flow calculation in IC engines, Internat. J. Numer. Methods Fluids 15 (1992) 693–714.

[13] W.M. Rohsenow, J.P. Hartnett, Handbook of Heat Transfer, McGraw-Hill, New York, 1973, pp. 9–2.

[14] A. Yoshizawa, K. Horiuti, Statistically-derived subgrid-scale kinetic energy model for the large-eddy simulation of turbulent flows, J. Phys. Soc. Japan 54 (8) (1985) 2834–2839.

[15] J.R. Smith, An accurate Navier–Stokes solver with an application to unsteady flows. Ph.D. Thesis, West Virginia University, 1996.

[16] J. Smagorinsky, General circulation experiments with the primitive equations, Mon. Wea. Rev. 91 (1963) 99–164.

[17] U. Piomelli, High Reynolds number calculations using the dynamic subgrid scale stress model, Phys. Fluids A 5 (6) (1993) 1484–1490.

[18] S. Sakamoto, S. Murakami, A. Mochida, Numerical study on flow past 2D square cylinder by large eddy simulation: Comparison between 2D and 3D computations, J. Wind Engrg. Indust. Aerodynam. 50 (1993) 61–68.

[19] K.Y. Huh, I.-P. Chang, J.K. Martin, A comparison of boundary layer treatments for heat transfer in IC engines, SAE Paper 900252, 1990.

[20] S.V. Patankar, Numerical Heat Transfer and Fluid Flow, McGraw-Hill, New York, 1980.

[21] J. Yang, P. Pierce, J.K. Martin, D.E. Foster, Heat transfer predictions and experiments in a motored engine, SAE Trans. 881314 97 (6) (1988) 1608–1622.

[22] T.-W. Kuo, V.K. Duggal, Modeling of in-cylinder flow characteristics—Effect of engine design parameters. Flows in internal combustion engines—II, in: T. Uzkan (Ed.), ASME (1984) 9–17.